

## Article

# Cathepsin B-Cleavable Polymeric Photosensitizer Prodrug for Selective Photodynamic Therapy: In Vitro Studies

Manish Jain <sup>1,2</sup>, Jordan Bouilloux <sup>3</sup>, Ines Borrego <sup>1</sup>, Stéphane Cook <sup>1,4</sup>, Hubert van den Bergh <sup>5</sup>, Norbert Lange <sup>3</sup>, Georges Wagnieres <sup>6</sup> and Marie-Noelle Giraud <sup>1,\*</sup>

- <sup>1</sup> Department EMC, Faculty of Sciences and Medicine, University of Fribourg, CH-1700 Fribourg, Switzerland; manishjain.cdri@gmail.com (M.J.); ines.borrego@unifr.ch (I.B.); stephane.cook@h-fr.ch (S.C.)
- <sup>2</sup> Pharmacology Division, University Institute of Pharmaceutical Sciences (UIPS), Panjab University, Chandigarh 160014, India
- <sup>3</sup> School of Pharmaceutical Sciences, Laboratory of Pharmaceutical Technology, Institute of Pharmaceutical Sciences of Western Switzerland, University of Geneva, Rue Michel-Servet 1, CH-1211 Genève, Switzerland; jordan.bouilloux@unige.ch (J.B.); norbert.lange@unige.ch (N.L.)
- <sup>4</sup> HFR Hôpital Fribourgeois, CH-1708 Fribourg, Switzerland
- <sup>5</sup> Medical Photonics Group, LCOM-ISIC, Swiss Federal Institute of Technology (EPFL), CH-1015 Lausanne, Switzerland; hubert.vandenbergh@epfl.ch
- <sup>6</sup> Laboratory for Functional and Metabolic Imaging, LIFMET, Swiss Federal Institute of Technology (EPFL), CH-1105 Lausanne, Switzerland; georges.wagnieres@epfl.ch
- \* Correspondence: marie-noelle.giraud@unifr.ch

**Abstract:** Cathepsin B is a lysosomal cysteine protease that plays an important role in cancer, atherosclerosis, and other inflammatory diseases. The suppression of cathepsin B can inhibit tumor growth. The overexpression of cathepsin B can be used for the imaging and photodynamic therapy (PDT) of cancer. PDT targeting of cathepsin B may have a significant potential for selective destruction of cells with high cathepsin B activity. We synthesized a cathepsin B-cleavable polymeric photosensitizer prodrug (CTSB-PPP) that releases pheophorbide a (Pha), an efficient photosensitizer upon activation with cathepsin B. We determined the concentration dependant uptake in vitro, the safety, and subsequent PDT-induced toxicity of CTSB-PPP, and ROS production. CTSB-PPP was cleaved in bone marrow cells (BMCs), which express a high cathepsin B level. We showed that the intracellular fluorescence of Pha increased with increasing doses (3–48  $\mu\text{M}$ ) and exerted significant dark toxicity above 12  $\mu\text{M}$ , as assessed by MTT assay. However, 6  $\mu\text{M}$  showed no toxicity on cell viability and ex vivo vascular function. Time-dependent studies revealed that cellular accumulation of CTSB-PPP (6  $\mu\text{M}$ ) peaked at 60 min of treatment. PDT (light dose: 0–100  $\text{J}/\text{cm}^2$ , fluence rate: 100  $\text{mW}/\text{cm}^2$ ) was applied after CTSB-PPP treatment (6  $\mu\text{M}$  for 60 min) using a special frontal light diffuser coupled to a diode laser (671 nm). PDT resulted in a light dose-dependent reduction in the viability of BMCs and was associated with an increased intracellular ROS generation. Fluorescence and ROS generation was significantly reduced when the BMCs were pre-treated with E64-d, a cysteine protease inhibitor. In conclusion, we provide evidence that CTSB-PPP showed no dark toxicity at low concentrations. This probe could be utilized as a potential imaging agent to identify cells or tissues with cathepsin B activity. CTSB-PPP-based PDT results in effective cytotoxicity and thus, holds great promise as a therapeutic agent for achieving the selective destruction of cells with high cathepsin B activity.

**Keywords:** cathepsin B; photosensitizer; photodynamic therapy; prodrug



**Citation:** Jain, M.; Bouilloux, J.; Borrego, I.; Cook, S.; van den Bergh, H.; Lange, N.; Wagnieres, G.; Giraud, M.-N. Cathepsin B-Cleavable Polymeric Photosensitizer Prodrug for Selective Photodynamic Therapy: In Vitro Studies. *Pharmaceuticals* **2022**, *15*, 564. <https://doi.org/10.3390/ph15050564>

Academic Editor: Céline Frochet

Received: 4 April 2022

Accepted: 27 April 2022

Published: 30 April 2022

**Publisher's Note:** MDPI stays neutral with regard to jurisdictional claims in published maps and institutional affiliations.



**Copyright:** © 2022 by the authors. Licensee MDPI, Basel, Switzerland. This article is an open access article distributed under the terms and conditions of the Creative Commons Attribution (CC BY) license (<https://creativecommons.org/licenses/by/4.0/>).

## 1. Introduction

Proteases such as cathepsins, or matrix metalloproteinases, are upregulated in various pathologies and are potential therapeutic targets. In particular, cathepsin B (CTSB) overexpression is associated with metastatic cancer [1], atherosclerotic plaques [2], neurodegenerative diseases [3], and other inflammatory diseases, including COVID-19 [4]. CTSB

is a lysosomal cysteine protease involved in the degradation of proteins and organelles, antigen presentation, and autophagy [5]. In physiological conditions, it is highly regulated. The dysregulation of cathepsin B causes cells to acquire pathological phenotypes. In recent years, strategies have been proposed for the selective targeting of cysteine proteases, including the use of synthetic small molecule inhibitors or antibodies directed against cathepsins [6–9]. Nevertheless, most synthetic inhibitors usually have low bioavailability and often exert reactivity toward off-target proteins [10].

Photodynamic therapy (PDT) utilizes photosensitizer (PS), which upon activation via a light of a specific wavelength, generates cytotoxic ROS [11] that leads to cell death via the loss of mitochondrial membrane potential, lipid peroxidation, or protein denaturation of cellular membranes and organelles [12,13]. PDT presents a promising alternative for pathologies associated with vascular abnormalities, inflammatory processes, and the development of neoplasia [14]. To selectively target the cells overexpressing CTSB, we developed a cathepsin B-cleavable polymeric PS prodrug (CTSB-PPP). CTSB-PPP consists of a poly-L-lysine backbone, to which multiple copies of the PS ‘pheophorbide a’ (Pha) units are tethered via a cathepsin B-cleavable short peptide sequence.

Pha is a chlorin-based PS that has demonstrated a beneficial effect against leukaemia, colon cancer, uterine carcinosarcoma, and rheumatoid arthritis [15,16]. Several photosensitizers have been approved for clinical applications or under clinical trials [17]. Photofrin<sup>®</sup> (Axcan Pharma, Canada) is the first type to be clinically approved photosensitizer for the treatment of cancer. The second generation photosensitizers, such as Temoporfin (Foscan<sup>®</sup>, Biolitec, Germany), Motexafin lutetium, Palladium bacteriopheophorbide (TOOKAD<sup>®</sup>, Negma-Lerads), Purlytin<sup>®</sup>, Verteporfin (Visudyne<sup>®</sup>, Novartis, Switzerland), and Talaporfin (Laserphyrin<sup>®</sup>, Meiji Seika, Japan) are clinically approved or under-clinical trials. However, PDT using a conventional photosensitizer has disadvantages such as photosensitive side effects, low light penetration depth, inconvenience, and relatively high cost. In contrast, Pha is a promising photosensitizer for PDT that meets most of the criteria that a good photosensitizer should satisfy [18]. In a comparative study, Djalil A.D. et. al. [19] reported that the drug concentration that causes a 50% reduction in cell viability (the LC50) of pheophorbide-a was much lower (<5 $\mu$ M) than that of Protoporphyrin IX, suggesting a higher dose of the former. When used for diagnosis, *in vitro* studies demonstrated that Pha showed almost five times more fluorescence brightness than chlorin-e6 [20]. Pha thus provides a better signal-to-noise ratio with a better detection limit, which is a critical factor required for imaging probes.

Fluorescence emission and phototoxicity of the Pha units in the CTSB-PPP molecule are quenched via the “switch-off state” due to the close proximity of the rather lipophilic Pha molecules. Photoexcitation of CTSB-PPP thus leads to exciplex formation and quenching via internal conversion. In the target tissue, after proteolytic cleavage of the peptide sequence, the inactive PS becomes active, increasing the distance between the Pha molecules, i.e., the “switch-on state” [10,21–24]. These active PS can fluoresce upon activation via light of an appropriate wavelength (~670 nm in case of Pha), in the presence of molecular oxygen, leading to the generation of reactive oxygen species (ROS) that locally destroys cells over short diffusion distances [25].

The present work aims at (1) synthesizing a novel Pha-based CTSB-PPP, (2) investigating its safety using two different models, one *in vitro* and one *ex vivo*, and (3) assessing the *in vitro* efficacy of CTSB-PPP-based PDT. For *in vitro* studies, bone marrow cells (BMC) were chosen as a model, as they express a high content of CTSB.

## 2. Materials and Methods

### 2.1. Chemicals

Penicillin/Streptomycin, Trypsin-EDTA, Methylene tetrazolium (MTT), dihydroethidium (DHE), 1-ethyl-(3-dimethylaminopropyl)carbodiimide hydrochloride (EDC), 4-dimethylaminopyridine (DMAP), *N*-hydroxysuccinimide (NHS), poly-L-Lysine (PLL, 25 kDa), and other fine chemicals were obtained from Sigma (Buchs, Switzerland). Antibodies including

CD90, CD44, CD29, and E-64d were purchased from Abcam (Cambridge, UK). Cathepsin B polyclonal antibody (USCPAC964Mu01) was purchased from Chemie Brunschwig (Basel, Switzerland). Dulbecco's Modified Eagle Medium (DMEM) was purchased from vWR International (Nyon, Switzerland). Pheophorbide a (Pha) was purchased from Frontier Scientific (Logan, UT, USA). GAGRRAAG peptide was obtained from Caslo Laboratory (Lyngby, Denmark). mPEG-NHS 20 kDa was purchased from NANOCS (New York, NY, USA). *O*-(7-azabenzotriazole-1-yl)-*N,N,N',N'*-tetramethyluronium hexafluorophosphate (HATU) was obtained from GenScript Corporation (Piscataway, NJ, USA). Trifluoroacetic acid (TFA, 99%), *N,N'*-diisopropylethylamine (DIPEA), *N,N'*-dimethylformamide (DMF), and dimethylsulfoxide (DMSO) were obtained from Acros Organics (Thermo Fisher Scientific, Wohlen, Switzerland). *N*-succinimidyl(1-methyl-3-pyridinio)formate iodide was synthesized according to the literature [26]. Pha-NHS was prepared as described previously [27].

## 2.2. Synthesis and Characterization of CTSB-PPP

### 2.2.1. Synthesis of Pha-CTSB

Pha-NHS (20 mg,  $2.9 \times 10^{-5}$  moles), cathepsin B-cleavable peptide sequence, i.e., GAGRRAAG (TFA salt) (48 mg,  $5.8 \times 10^{-5}$  moles) [28] and DIPEA (20.2  $\mu$ L,  $1.2 \times 10^{-4}$  moles) were stirred in DMF (10 mL) under argon in the dark at room temperature overnight. H<sub>2</sub>O (10 mL) and TFA (30  $\mu$ L) were added to reach pH = 4. Solvents were removed under reduced pressure, and the crude product was purified by semi-preparative reversed-phase high-performance liquid chromatography (RP-HPLC) on an automatic PuriFlash 4100 instrumentation with an Interchim Soft version 5.0x software from Interchim (Montluçon, France). Separation was achieved on a Nucleodur<sup>®</sup> C<sub>18</sub> HTec column (762,556.210; 5  $\mu$ m, 21  $\times$  250 mm) from Macherey-Nagel (Oensingen, Switzerland) with one of the following systems: 9 mL/min, 30–100% solvent B in 30 min (with H<sub>2</sub>O + 0.01% TFA as solvent A and ACN + 0.01% TFA as solvent B), detection at 210, 313 and 410 nm. The final product was then lyophilized to give a green solid (33.2 mg, 88.8% yield). <sup>1</sup>H NMR (300 MHz, DMSO-*d*<sub>6</sub>)  $\delta$  12.60 (s, 1H), 9.82 (s, 1H), 9.48 (s, 1H), 8.90 (d, *J* = 16.0 Hz, 1H), 8.33–7.85 (m, 10H), 7.44 (d, *J* = 5.6 Hz, 2H), 6.48–6.32 (m, 2H), 6.24 (dd, *J* = 11.6, 1.6 Hz, 1H), 4.57 (q, *J* = 6.8 Hz, 1H), 4.26 (dq, *J* = 18.1, 7.1 Hz, 6H), 4.04 (d, *J* = 8.2 Hz, 1H), 3.87–3.56 (m, 17H), 3.43 (d, *J* = 11.3 Hz, 4H), 3.26 (d, *J* = 12.3 Hz, 7H), 3.11–3.01 (m, 5H), 2.48–2.39 (m, 1H), 2.36–2.25 (m, 1H), 2.22 (s, 6H), 2.09 (d, *J* = 12.1 Hz, 1H), 1.77 (d, *J* = 7.1 Hz, 3H), 1.63 (h, *J* = 7.9, 6.4 Hz, 6H), 1.46 (s, 9H), 1.18 (ddd, *J* = 14.9, 6.7, 3.0 Hz, 11H), 0.47 (s, 1H), –1.79 (s, 1H). ESI-MS: *m/z* 1290.3 [M + H]<sup>+</sup>; 645.8 [M + 2H]<sup>2+</sup>.

### 2.2.2. Synthesis of CTSB-PPP

PLL (25 kDa, 9.42 mg,  $3.9 \times 10^{-7}$  moles,  $4.5 \times 10^{-5}$  moles of -NH<sub>2</sub> functions) was added to a solution of Pha-CTSB (16.3 mg,  $1.26 \times 10^{-5}$  moles, 28% of the -NH<sub>2</sub> functions of the PLL backbone) and HATU (6.54 mg,  $1.72 \times 10^{-5}$  moles, 1.3 equivalents of the Pha-CTSB to be activated) in DMSO (3 mL). Following activation, DIPEA (45  $\mu$ L,  $2.58 \times 10^{-4}$  moles) was added to the mixture, which was then stirred under argon, and the reaction was allowed to proceed in the dark overnight. mPEG-NHS (20 kDa, 9.93 mg,  $4.95 \times 10^{-5}$  moles, 1% of the -NH<sub>2</sub> functions of the PLL backbone, 1.1 equivalent) and DIPEA (15  $\mu$ L) in DMSO (1.5 mL) were added to the mixture, and the reaction was allowed to proceed in the dark overnight. Remaining free -NH<sub>2</sub> functions of the PLL backbone were capped with *N*-succinimidyl(1-methyl-3-pyridinio)formate iodide (12.75 mg,  $3.51 \times 10^{-5}$  moles, 71%, 1.1 equivalent) and DIPEA (15  $\mu$ L) in DMSO (1.2 mL), and the reaction was allowed to proceed in the dark overnight. The reaction was quenched by adding a mixture of water and TFA to reach pH = 3. Solvents were removed under reduced pressure, and the crude was purified by size exclusion chromatography (SEC) using a Sephacryl<sup>™</sup> S-100 column (Amersham Biosciences, Otelfingen, Switzerland) and H<sub>2</sub>O/ACN/TFA (70:30:0.01) as the eluting solvent (1.2 mL/min). The final product was lyophilized to give a green solid (31.3 mg, 80.4% yield).

### 2.3. Quenching Efficiency

The corresponding polymer carrying only 1% of peptide-Pha was prepared to assess the quenching efficiency. To this end, PLL (25 kDa, 22.93 mg,  $9.17 \times 10^{-7}$  moles,  $1.10 \times 10^{-4}$  moles of  $-NH_2$  functions) was added to a solution of Pha-CTSB (1.41 mg,  $1.09 \times 10^{-6}$  moles, 1% of the  $-NH_2$  functions of the PLL backbone) and HATU (0.58 mg,  $1.52 \times 10^{-6}$  moles, 1.3 equivalents of the Pha-CTSB to be activated) in DMSO (1 mL). DIPEA (60  $\mu$ L,  $3.44 \times 10^{-4}$  moles) was then added to the mixture, which was then stirred under argon, and the reaction was allowed to proceed in the dark overnight. mPEG-NHS (20 kDa, 24.16 mg,  $1.21 \times 10^{-6}$  moles, 1% of the  $-NH_2$  functions of the PLL backbone, 1.1 equivalent) and DIPEA (10  $\mu$ L,  $5.74 \times 10^{-5}$  moles) in DMSO (1 mL) were added to the mixture, and the reaction was allowed to proceed in the dark overnight. The remaining free  $-NH_2$  functions of the PLL backbone were capped with *N*-succinimidyl(1-methyl-3pyridinio)formate iodide (42.91 mg,  $1.18 \times 10^{-4}$  moles, 98%, 1.1 equivalent) and DIPEA (10  $\mu$ L,  $5.74 \times 10^{-5}$  moles) in DMSO (1 mL), and the reaction was allowed to proceed in the dark overnight. The reaction was quenched by adding a mixture of water and TFA to reach pH = 3. Solvents were removed under reduced pressure, and the crude was purified by SEC using a Sephacryl<sup>TM</sup> S-100 column (Amersham Biosciences, Otelfingen, Switzerland) and H<sub>2</sub>O/ACN/TFA (70:30:0.01) as the eluting solvent (1.2 mL/min). The final product was then lyophilized to give a green solid.

### 2.4. Spectral Characterization

The absorbance and emission spectra of CTSB-PPP and its reference conjugate grafted with 1% Pha-peptide (3  $\mu$ M Pha equivalent) were measured at 37 °C using a Biotek Multiplate reader (Synergy 2, Biotek, Winooski, VT, USA), setting the excitation at 400 nm and emission at 670 nm. The gain was set to 100, and the slit width was 9, with an accumulative number of 5. Five samples of both conjugates were prepared and measured in the 96-well quartz plate. The fluorescence quenching factor (*x*-fold decrease in background subtracted fluorescence at the 670 nm emission maximum) was calculated with respect to the non-quenched reference conjugate.

### 2.5. Animal Experimentation

Seven-week-old male Lewis rats were used in the present study. The animals were obtained from Charles River Laboratories, France. All the procedures involving animal experimentation were performed in compliance with the European Convention on Animal Care in accordance with the Swiss Animal Protection Law after obtaining permission from the State Veterinary Office, Fribourg, and approved by the Swiss Federal Veterinary Office, Switzerland (FR 2013-35). The animals were housed in individually ventilated cages and were maintained on a chow diet, water ad libitum, and 12 h/12 h light-dark cycle.

### 2.6. Cell Culture Conditions

BMCs were isolated from the bone marrow of a male Lewis rat and cultured in 75 cm<sup>2</sup> containing Dulbecco's Modified Eagle Medium supplemented with 10% Fetal Bovine Serum and 1% Penicillin/Streptomycin. BMCs were selected upon adherence, and the culture medium was removed after 2 days to remove non-adherent cells. The medium was subsequently replaced after 3 days, and the BMCs were allowed to grow for 8–10 days to reach confluence [29]. The cells were harvested using Trypsin-EDTA and were sub-cultured at a density of  $2.1 \times 10^6$  cells in a 75 cm<sup>2</sup> flask. BMCs were characterized by flow cytometry for the presence of surface markers CD90, CD44, and CD29 using specific antibodies [30]. All experiments were performed on confluent cells within passages of 3–4.

### 2.7. In Vitro Activation of CTSB-PPP

BMCs were seeded into 48-well plates at a density of  $10^5$  cells per well and then cultured in the medium for 24 h to attach. To evaluate the dose-dependent cellular activation of CTSB-PPP, cells were washed and treated overnight, with or without E-64d (50  $\mu$ M). Cells

were washed with PBS, and solutions of CTSB-PPP in DMEM at final concentrations of 6, 12, 24, or 48  $\mu\text{M}$  of Pha equivalents were added for 60 min. In another set of experiments, cells were treated with 6  $\mu\text{M}$  CTSB-PPP for 10 min, 20 min, 60 min, or 24 h. Following treatment, cells were immediately washed twice. The cellular localization of CTSB-PPP was visualized using a confocal microscope (Leica TCS SP5 DMI6000) equipped with a Leica plan apo 20 $\times$  (numerical aperture 0.7) dry objective. Red fluorescence of the PS and corresponding bright-field images were collected in the fluorescence emission range of 670–700 nm using a 405 nm diode laser for excitation [31,32]. Pictures were taken using Leica Application Suite Advanced Fluorescence (LASAF) software (Leica Microsystems). Fluorescence intensity per cell was quantified using the ImageJ, software as previously described [33,34].

### 2.8. MTT Assay

To assess the dark toxicity of CTSB-PPP, BMCs were seeded into 96-well plates at a density of  $2 \times 10^3$  cells/well and were allowed to adhere overnight. Cells were then treated with the indicated concentration of CTSB-PPP, in the presence or absence of E-64d, for 60 min. Subsequently, cells were washed and returned to the incubator, and viability was evaluated after 24 h by MTT assay. Briefly, cells were incubated with MTT (20  $\mu\text{L}$ , 5 mg/mL in PBS) at 37  $^\circ\text{C}$  for 4 h. After incubation, the formazan product was dissolved in DMSO, and absorbance was read at 570 nm using an ELISA plate reader. The percentage of cell metabolic activity as an indicator of cell viability was calculated with respect to control samples as: (% cell viability = (mean OD value of the irradiated cells/mean OD value of the non-irradiated cells)  $\times$  100) [35,36].

### 2.9. Light Source and PDT

PDT efficacy was determined in BMCs treated with or without CTSB-PPP (6  $\mu\text{M}$ ). Immediately after one hour of treatment, cells were illuminated with red light using a frontal light diffuser (FD-1, Medlight SA, Switzerland) coupled to a 1W Diode laser (Frankfurt Laser Company, Germany) emitting at 671 nm. This diffuser has a graded-index lens at its distal end and two perpendicular mode scramblers to give nearly perfect homogenous light intensity distinguished over a large circular area. Laser power emitted by the frontal light diffuser was calibrated with a power meter (Spectra-Physics Newport; model 407A) according to a procedure described in detail by Borle et al. [37]. The light diffuser was placed 1 cm away from the bottom of the well, and total light doses ranging from 0 J/cm<sup>2</sup> to 200 J/cm<sup>2</sup> were applied at a fluence rate of 100 mW/cm<sup>2</sup> [23,38]. After PDT, MTT assays were performed to assess the cell viability, as described above.

### 2.10. Detection of ROS

Cellular ROS was detected by DHE staining. Immediately after PDT, cells were rinsed with PBS and incubated with DHE (10  $\mu\text{M}$ ) in a dark, humidified chamber for 10 min at 37  $^\circ\text{C}$ . Cells were washed with PBS and counterstained with Hoechst (5  $\mu\text{g}/\text{mL}$ ) [39]. Fluorescent images were acquired with the same exposure time from different groups on a Nikon Ni-U microscope (Nikon, Tokyo, Japan). DHE fluorescence intensity normalized with the area was measured using ImageJ software and is expressed as DHE fluorescence intensity per  $\mu\text{m}^2$  (arbitrary units).

### 2.11. Assessment of Vascular Function

Aortic segments from C57BL/6J were cut into rings (2 mm in length) and mounted between two L-shaped hooks in a Multi-Myograph System (Model 720 MO, Danish Myo Technology A/S, Denmark). Myograph chambers were filled with Krebs bicarbonate buffer and were bubbled with 95% O<sub>2</sub> and 5% CO<sub>2</sub> at 37  $^\circ\text{C}$ . After equilibration, the aortic rings were exposed to KCl Krebs buffer (80 mM) to assess the maximum tissue contractility. Changes in isometric tension ( $\Delta$  mN) were recorded with Lab Chart Pro v8.0.5 software (AD Instruments, UK). The vasoconstriction response to phenylephrine (PE) was deter-



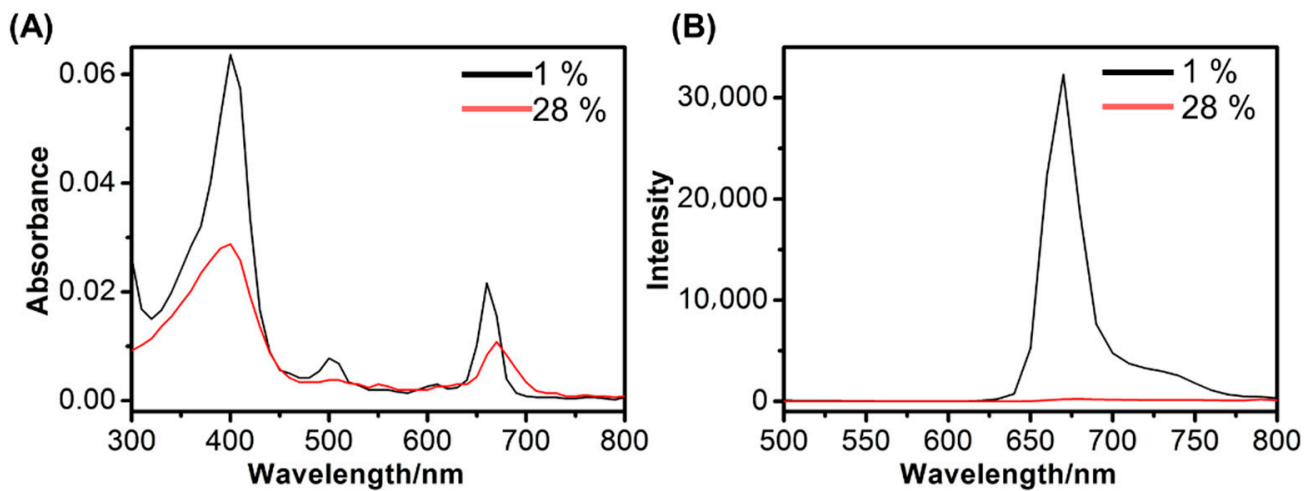


**Figure 2.** Fluorescence spectra of CTSB-PPP. (A) absorption spectra and (B) Emission spectra of CTSB-PPP (28% loading of Pha-peptide) and its non-quenched reference (1% loading of Pha-peptide) with equimolar amount of Pha (3.0  $\mu$ M) in aqueous DPBS buffer. Ex = 400 nm; Em = 670 nm; T = 37  $^{\circ}$ C.

### 3.2. Cellular Uptake, Specificity, and Dark Toxicity of CTSB-PPP

After entering the cells, the peptide linker GAGRRAAG is cleaved by cathepsin B, releasing free Pha that can be detected via fluorescence imaging. First, the expression of cathepsin B in BMCs was confirmed by immunostaining (Supplementary Figure S1). Then, the uptake efficiency of CTSB-PPP within BMCs was examined after one hour of treatment using confocal microscopy (Figure 3A). The presence of a Pha-derived red fluorescence signal in cells treated with CTSB-PPP reflected the activation of the probe within the cell. The quantification of the fluorescence intensity (FI) revealed a dose-dependent increase in the accumulation of CTSB-PPP. Compared to background auto-fluorescence from control cells (FI =  $278 \pm 38$ ), FI was significantly higher in cells treated with CTSB-PPP at a 6  $\mu$ M concentration ( $4174 \pm 502$ ) or 12  $\mu$ M ( $4834 \pm 906$ ). A further significant increase in FI was noted by increasing the concentration to 24  $\mu$ M ( $6841 \pm 948$ ). However, no further change in FI was noted in BMCs treated with 48  $\mu$ M CTSB-PPP ( $7235 \pm 1241$ ) (Figure 3C, Supplementary Table S1). The safety of CTSB-PPP was also investigated in parallel by examining its dark cytotoxicity. BMCs were treated for 1 h, with or without 6, 12, or 24  $\mu$ M CTSB-PPP. When compared to the control ( $100 \pm 14.9\%$ ), CTSB-PPP treatment at 6  $\mu$ M concentration did not exert any significant loss in cell viability ( $89.7 \pm 19.5\%$ ), as determined by MTT assay. However, a significant reduction in cell viability was noted at higher concentrations of CTSB-PPP, i.e., 12  $\mu$ M ( $71.7 \pm 7.9\%$ ) and 24  $\mu$ M ( $57.0 \pm 15.4\%$ ) (Figure 3D). To define the specificity of CTSB-PPP, BMCs were treated with E-64d (an irreversible cell-permeable cysteine protease inhibitor) (Figure 3B). Pre-treatment with E-64d (50  $\mu$ M) led to a significant reduction in FI of CTSB-PPP at 6  $\mu$ M ( $2114 \pm 705$ ) or 12  $\mu$ M concentration ( $2837 \pm 395$ ), as compared to their cells without E-64d (Figure 3C).

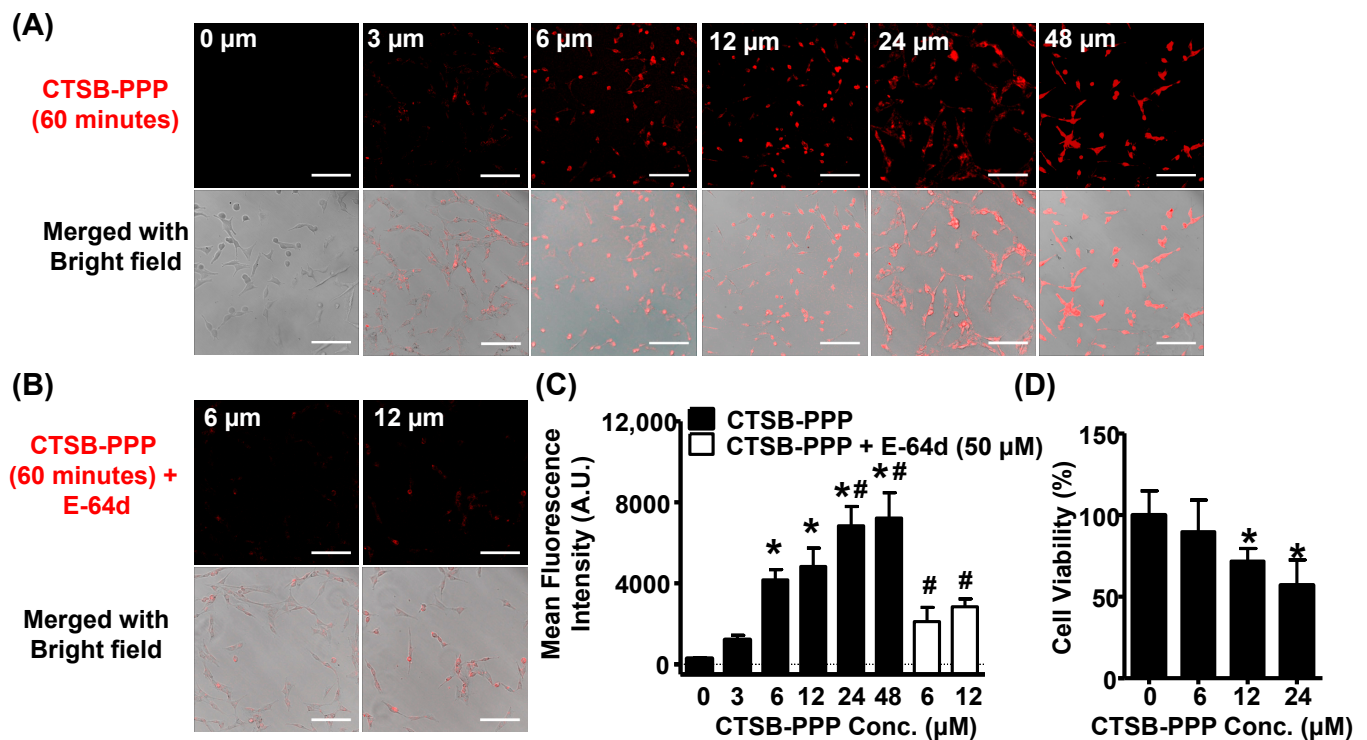


**Figure 3.** Dose-dependent cellular accumulation of CTSB-PPP. (A,B) BMCs were treated for 1 h with CTSB-PPP at different concentrations, in the presence or absence of E-64d, and intracellular accumulation was monitored by confocal microscopy. The upper panel illustrates characteristic fluorescence of cleaved PS consisting of Pha as fluorophore in red, and the lower panel is merged with corresponding bright field images, illustrating localization. Scale bar: 100 μm. (C) Bar diagram representing quantification of fluorescence intensity per cell in each group ( $n = 3$ ), and (D) BMCs were treated with varying concentration of CTSB-PPP for 1 h. Cell viability was detected by MTT assay after 24 h of treatment ( $n = 3$ ). \*  $p < 0.05$  vs. vehicle treated i.e., 0 μM CTSB-PPP treated cells; #  $p < 0.05$  vs. 6 or 12 μM CTSB-PPP treated cells. Statistical analysis—one-way ANOVA, followed by Bonferroni's post hoc test.

### 3.3. Time-Dependent CTSB-PPP Accumulation

To assess the PDT efficacy of CTSB-PPP, we first identified the optimal time required by CTSB-PPP to accumulate in BMCs. BMCs were treated with CTSB-PPP 6 μM (non-toxic dose) for different times, and FI was quantified on corresponding fluorescent images (Figure 4A). A sharp increase in FI, representing activation and accumulation of the CTSB-PPP probe, was noted as early as 10 min ( $1932 \pm 496$ ), which slightly increased at 20 min ( $2211 \pm 222$ ) and peaked at 60 min of treatment ( $3585 \pm 505$ ). Increasing the treatment time to 24 h resulted in a slight reduction in fluorescence ( $3045 \pm 262$ ) (Figure 4B, Supplementary Table S2).

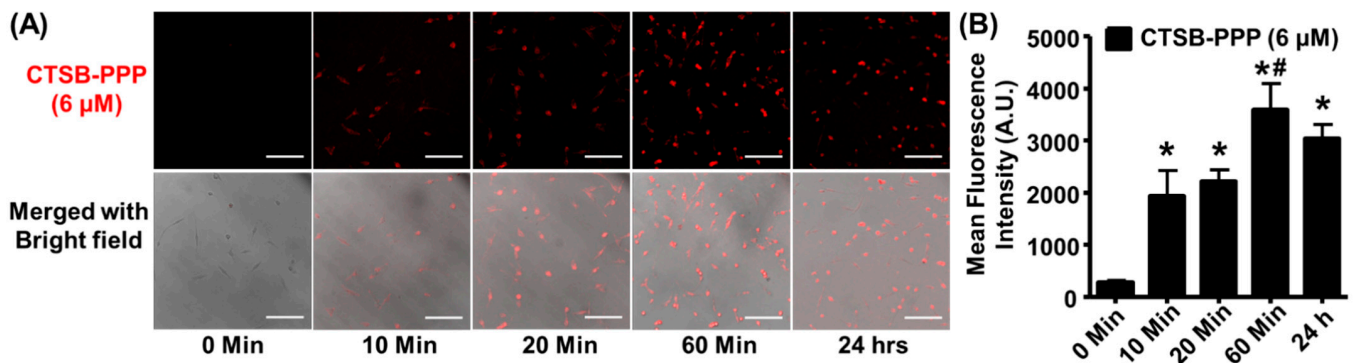


**Figure 4.** Time-dependent activation and accumulation of CTSB-PPP. (A) Confocal fluorescence micrographs merged with corresponding bright field images of BMCs treated with 6 μM CTSB-PPP for 10 min, 20 min, 60 min, or 24 h. Scale bar: 100 μm. (B) Bar graph representing the fluorescence intensity per cell in each group (n = 3). \* p < 0.05 vs. 10 min, # p < 0.05 vs. 20 min. Statistical analysis—one-way ANOVA, followed by Bonferroni's post hoc test.

3.4. Ex Vivo Toxicity

We assessed the effect of CTSB-PPP (6 μM) on vascular function using a Myogram. KCl induced maximal tissue contractility, dose-dependent phenylephrine (PE) induced contraction, and acetylcholine (ACh) induced relaxation were determined before and after CTSB-PPP treatment (6 μM for 1 h). The KCl response, PE induced maximal contraction, and ACh-induced endothelium-dependent relaxation were not altered after CTSB-PPP treatment (Figure 5A), suggesting that CTSB-PPP per se has no toxic effect on vascular function. We also confirmed the activation of CTSB-PPP ex vivo. As shown in Figure 5B, Pha was observed in the endothelium of the aortic ring.

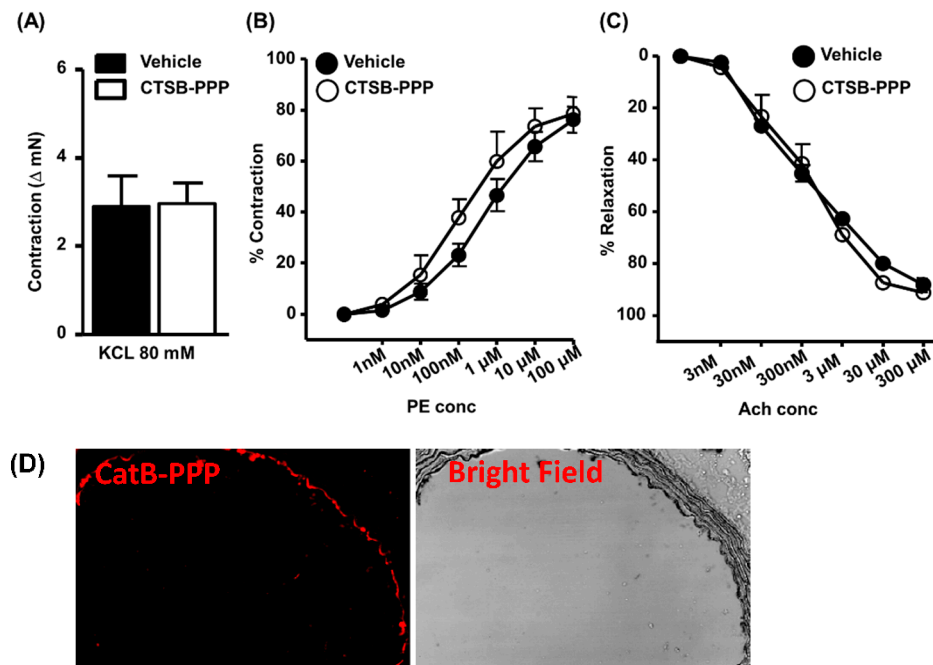


**Figure 5.** CTSB-PPP itself does not affect vascular function. Aortic segments from C57BL/6J mice were mounted in Myograph. Vascular function was assessed before or after CTSB-PPP (6 μM for 1 h)

treatment (A) Bar diagram representing KCl induced contraction, (B) Dose-dependent phenylephrine (1 nM–100  $\mu$ M) induced contractions, Scale bar: 100  $\mu$ m, and (C) Acetylcholine (3 nM–300  $\mu$ M) mediated relaxations ( $n = 4$ ). Statistical analysis—unpaired two-tailed Student's *t*-test. (D) CTSB-PPP (6  $\mu$ M for 1 h) was perfused ex vivo through the thoracic aorta isolated from wild type C57Bl/6J mice. Representative images showing characteristic fluorescence of cleaved PS consisting of Pha as fluorophore in red, along with corresponding bright field images of aortic sections.

### 3.5. CTSB-PPP Based PDT Efficacy

BMCs, treated with or without CTSB-PPP (6  $\mu$ M for 1 h), were irradiated with a light dose of 0 to 100 J/cm<sup>2</sup>. Light doses up to 100 J/cm<sup>2</sup> did not exert any significant change on cell viability; however, at 200 J/cm<sup>2</sup>, cell viability was reduced to 37.6  $\pm$  2.4%, as compared to the control non-illuminated cells (100  $\pm$  14.1%) (Figure 6A). A drastic reduction in cell viability was observed in cells treated with CTSB-PPP (6  $\mu$ M for 1 h) and illuminated with 12.5 (54.1  $\pm$  7.5%), 25 (51.2  $\pm$  6.8%), 50 (35.2  $\pm$  3.4%), or 100 J/cm<sup>2</sup> (32.5  $\pm$  3.4), as compared to non-illuminated cells treated with the same dose of CTSB-PPP (95.0  $\pm$  5.1%) (Figure 6B).

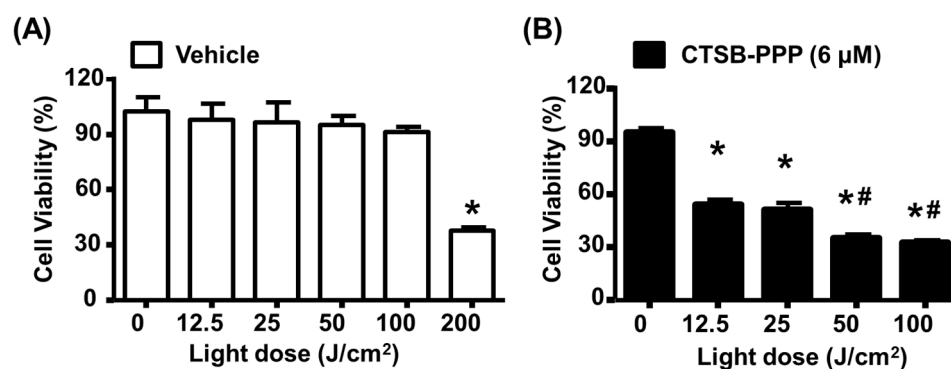


**Figure 6.** PDT-induced photo toxicity. BMCs were treated, with or without CTSB-PPP (6  $\mu$ M), for 1 h. PDT was applied immediately after treatment. Cell viability was determined after 24 h by MTT assay. Bar diagram representing (A) effect of different dose of laser irradiation on the viability of BMCs and (B) phototoxicity of CTSB-PPP illuminated with red light at fluence of 12.5 J/cm<sup>2</sup> ( $n = 3$ ). \*  $p < 0.05$  vs. vehicle treated non-illuminated control cells. #  $p < 0.05$  vs. 12.5 or 25 J/cm<sup>2</sup> treated cells. Statistical analysis—one-way ANOVA, followed by Bonferroni's post hoc test.

### 3.6. PDT with CTSB-PPP Stimulated ROS Generation

It is well accepted that PDT utilizes light to excite a PS and generate cytotoxic ROS [14]. Therefore, we determined whether the phototoxic effect of CTSB-PPP was associated with ROS production. ROS levels were determined immediately after PDT using DHE staining (Figure 7A). DHE fluorescence intensity (arbitrary units) was not significantly changed in only CTSB-PPP-treated (46,194  $\pm$  30,346) or only laser-irradiated groups (44,100  $\pm$  35,834), as compared to the vehicle-treated control (22,370  $\pm$  22,288). A significant increase in ROS levels was observed in CTSB-PPP photo-irradiated cells (20,2475  $\pm$  32,952) compared to vehicle-treated control. Pre-treatment with E-64d (50  $\mu$ M) led to a significant reduction in cellular ROS levels of CTSB-PPP photo-irradiated cells (86,686  $\pm$  40,420) (Figure 7B, Supplementary Table S3). Original fluorescent photomicrograph of DHE staining, along with Hoechst staining, are presented in Supplementary Figure S2.

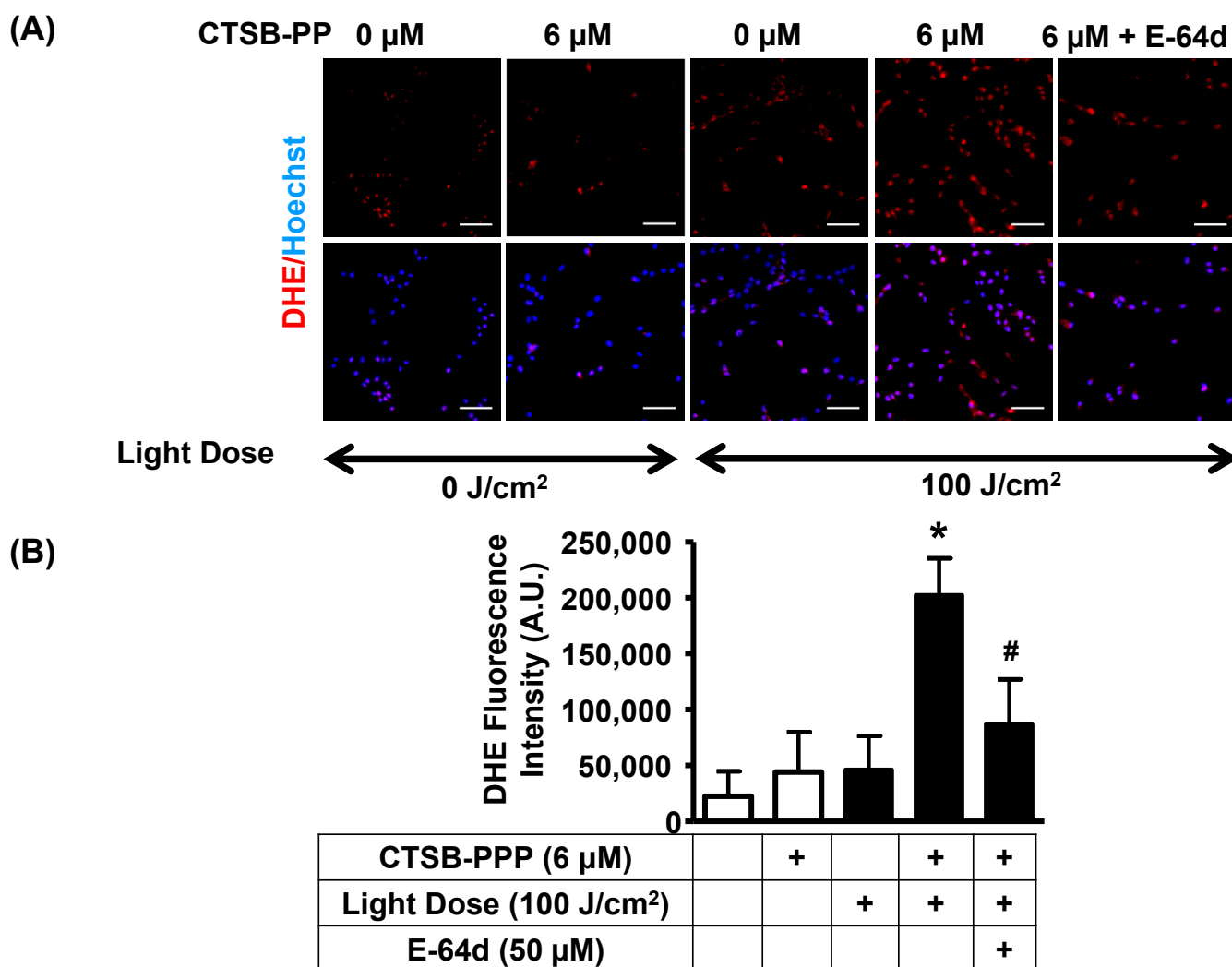


**Figure 7.** ROS production by CTSB-PPP-mediated PDT. ROS levels were determined immediately after PDT by DHE staining (A) Upper-top panel show a representative fluorescent photomicrograph of DHE staining, indicating ROS signals as red fluorescence, and upper-bottom panel represents the merged image with Hoechst in blue. Scale bar: 100  $\mu\text{m}$ . (B) Bar diagram representing DHE fluorescence intensity/ $\mu\text{m}^2$ . \*  $p < 0.05$  vs. vehicle-treated, un-illuminated control. #  $p < 0.05$  vs. CTSB-PPP-treated photo-illuminated cells. Statistical analysis—one-way ANOVA, followed by Bonferroni's post hoc test.

#### 4. Discussion

We developed a new hydrophilic PS prodrug to selectively target cathepsin B, which is highly upregulated in several pathologies, including immune disorders, cardiovascular diseases, and cancer. Our results demonstrated that the fluorescence of the prodrug was efficiently quenched in the prodrug's native state. Intracellular activation of the prodrug in BMCs, following the selective cleavage of the peptide linker by cathepsin B, restores photoactivity of the Pha, which can be imaged and quantified by microscopy. The photoactivation of CTSB-PPP also resulted in the efficient reduction in BMCs viability. The probe can thus target upregulated cathepsin B protease activity and is, therefore, a very selective theranostic molecule.

In the current study, we have used the GAGRRAAG peptide sequence, which was designed from the AGRRAA sequence identified as a CTSB-specific substrate by Ruzza et al. [28]. Two G residues (at the amino- and carboxyl-end) were added for further chemical modification. Previously, we have also shown the proteolytic cleavability of the GAGRRAAG

peptide linker using CTSB from a human placenta [24]. CTSB-sensitive PPP contains multiple copies of Pha as the PS. Pha is a product of chlorophyll breakdown and, upon photo-illumination at around 666 nm, it induces apoptosis and necrosis in cells via the generation of ROS and the release of cytochrome c [44,45]. Besides this known toxicological profile, the strong absorption band at 666 nm allows relatively deep tissue penetration, thus making it a suitable PS for our prodrug strategy. The Pha moieties are linked to a poly-L-lysine backbone via a peptide sequence. Previously, we have showed that the coupling of varying amounts of pheophorbide a-NHS ester to PLL results in the complete disappearance of the peak corresponding to pheophorbide a-NHS ( $\lambda_{\text{abs}} = 400$  nm) and the appearance of a new, more polar, broad peak corresponding to PPP, thus providing conjugates with an estimated average of 1, 6, 12, 18, 24, and 30 PS units per polymer chain [27]. The fluorescence quenching factor increased as a function of the number of PS units in a polymer chain, revealing that at equimolar concentrations of the PS (equi-absorbant solutions at 667 nm), better fluorescence quenching is observed for higher PS loading [27]. Earlier, Ruzza et al. [28] showed that the specific sequence Arg-Arg-Ala-Ala exhibits the best selectivity for efficient enzymatic hydrolysis at lysosomal pH. Cleavage of the peptide linker by CTSB releases Pha, which could be detected at the excitation and emission maxima of 405 nm and 670 nm, respectively. In the present work, we have used 28% of PS-peptide loading per polymer chain [27,46], resulting in efficient fluorescence quenching.

The localization of a PS in sufficient concentration in a target tissue of interest is essential for the target's fluorescence detection and its selective removal by photodynamic action. We used BMCs to assess intracellular activation, dark toxicity, and PDT-induced cytotoxicity of CTSB-PPP, as they are known to express cathepsin B [46,47]. Our results showed the homogeneous activation of CTSB-PPP, indicating the degradation of the peptide linker resulting in the restoration of fluorescence. CTSB-PPP demonstrated dose-dependent accumulation, where the maximum accumulation appeared after about 1 h. Both active and/or passive diffusion processes may account for this accumulation. A slight reduction in fluorescence intensity observed at 24 h of treatment could be attributed to aggregation of the PS, resulting in a decrease in fluorescence. Previous reports have documented that both monomer and aggregated forms of PSs can be present in cells, where the aggregated state exhibits diminished fluorescence and photosensitizing efficiency [48,49]. The PS moiety used in CTSB-PPP is reported to exhibit significant dark toxicity on normal Vero cells at 10  $\mu\text{M}$  concentration, where the viability was reduced to 43% [19]. Therefore, we assessed whether the coupling of Pha to a polymeric chain could influence dark toxicity. Our study corroborates the Vero cell assay, as CTSB-PPP showed cytotoxicity at 12  $\mu\text{M}$ . Nevertheless, CTSB-PPP was safe at 6  $\mu\text{M}$  concentration (Pha equivalent).

Ex vivo toxicity provided further confirmation of the reliable safety of CTSB-PPP. Vascular function assays with isolated tissue baths evaluated the potential deleterious effect on aortic rings isolated from wild type mice. The primary advantage of this technique is that the tissue is living and functions as a whole tissue, with a physiological outcome (contraction or relaxation) that is relevant to the body [50]. Our results showed that vascular integrity was maintained, and CTSB had no deleterious effect on maximum tissue contractility and endothelium-dependent relaxation. Imaging of protease activity has been effectively utilized for in vivo diagnostic imaging of tumors, arthritis [51], cancer [52], and vulnerable atherosclerotic plaques [53]. Pheophorbide-a, in CTSB-PPP, is highly fluorescent in the near-infrared (NIR) spectrum. NIR shows lower photodamage effects, greater tissue penetration depth, and a higher signal-to-noise ratio than UV or visible light. Thus, the localized accumulation of CTSB-PPP in tissues with high protease activity, along with the fluorescence of pheophorbide-a, can be used in cancer bioimaging techniques. Altogether, our results suggest that CTSB-PPP may be a good candidate as a diagnostic tool due for the distinct expression profiling of CTSB in disease pathology.

PDT efficacy using CTSB-PPP was demonstrated in vitro. Significant reduction in cell viability upon photo-illumination showed an adequate photodynamic response. The active pheophorbide-a exerts cytotoxicity by several mechanisms, mainly based on apoptosis and

the autophagy pathway [18]. Pha-mediated PDT is known to upregulate the expression of BCL-2 (B-cell lymphoma-2), BAX (Bcl-2-associated X protein), Caspase-3, and PARP (poly adenosine diphosphate-ribose polymerase) [54]. In addition, it is also reported that pheophorbide-a based PDT reduces the phosphorylation of mTOR, which is involved in cancer cell proliferation [55]. These reports suggest that CTSB-PPP-based PDT may promote the signaling involved in cell apoptosis and inhibit the activation of mTOR to suppress cell proliferation.

Upon illumination, PS molecules generate hydroxyl radical, superoxide anion, hydrogen peroxide, and singlet oxygen. Singlet oxygen can further react with nearby molecules to induce the formation of other ROS species that can be detected via chemical sensors, such as DHE [39,56]. When ROS concentration surpasses a certain level, it leads to apoptosis via the loss of mitochondrial membrane potential, lipid peroxidation, or the protein denaturation of cellular membranes and organelles [12,13]. Our results demonstrate that CTSB-PPP in the absence of light does not induce ROS production, again confirming the absence of dark toxicity of the PS at the selected dose. The photo-illumination of CTSB-PPP led to a ~4-fold increase in ROS level, attributed to its efficient phototoxic effects.

## 5. Conclusions

CTSB-PPP showed no dark toxicity at low concentrations. This probe may thus be utilized as a potential imaging agent to identify cells or tissues with high cathepsin B protease activity. CTSB-PPP-based PDT results in effective cytotoxicity and therefore, holds promise as a therapeutic agent for achieving the highly selective destruction of cells with high proteolytic activity, for instance, in neoplasms. However, a more detailed in vivo study is required to establish proof of this concept for the CTSB-PPP-based selective targeting of cathepsin B.

**Supplementary Materials:** The following supporting information can be downloaded at: <https://www.mdpi.com/article/10.3390/ph15050564/s1>, Figure S1: Expression of Cathepsin B in BMCs; Figure S2: Original fluorescent photomicrograph of DHE and Hoechst staining; Supplementary Table S1: Related analysis for Figure 3A; Supplementary Table S2: Related analysis for Figure 4B; Supplementary Table S3: Related analysis for Figure 7.

**Author Contributions:** M.J., J.B., I.B., S.C., G.W., N.L. and M.-N.G. contributed to the design of the work; M.J., J.B. and I.B. performed the experiments; M.J. analysed the data and prepared the figures; M.J. and M.-N.G. wrote the main manuscript; H.v.d.B. and G.W. provided the light source and contributed to light dosimetry calculations; G.W. and H.v.d.B. provided critical inputs for review and editing of the manuscript; M.-N.G. and S.C. provided the resources. All authors have read and agreed to the published version of the manuscript.

**Funding:** This work was supported by the Swiss National Science Foundation Grant 150271, attributed to M.N.G., G.W., and S.C.; the Fonds Scientifique Cardiovasculaire F.S.C., Fribourg Hospital, attributed to S.C., and the Ramalingaswami Re-Entry Fellowship Grant from the Department of Biotechnology, Government of India (BT/RLF/Re-entry/28/2019), attributed to M.J.

**Institutional Review Board Statement:** The animal study protocol was approved by the Swiss Federal Veterinary Office, Switzerland (FR 2013-35).

**Informed Consent Statement:** Not applicable.

**Data Availability Statement:** All data is available in this manuscript and its accompanying supplementary information.

**Acknowledgments:** We greatly appreciate the Light Microscopy Facility at the University of Fribourg for its expert assistance in acquiring images with a confocal microscope. The authors would like to acknowledge the excellent technical assistance of Marie Larraillet. The graphical abstract was performed with Biorender.com.

**Conflicts of Interest:** The funders had no role in the design of the study; in the collection, analyses, or interpretation of data; in the writing of the manuscript, or in the decision to publish the results.

## References

1. Pollard, J.W. Tumour-educated macrophages promote tumour progression and metastasis. *Nat. Rev. Cancer* **2004**, *4*, 71–78. [[CrossRef](#)] [[PubMed](#)]
2. Hua, Y.; Nair, S. Proteases in cardiometabolic diseases: Pathophysiology, molecular mechanisms and clinical applications. *Biochim. Biophys. Acta* **2015**, *1852*, 195–208. [[CrossRef](#)]
3. Hook, V.; Yoon, M.; Mosier, C.; Ito, G.; Podvin, S.; Head, B.P.; Rissman, R.; O'Donoghue, A.J.; Hook, G. Cathepsin B in neurodegeneration of Alzheimer's disease, traumatic brain injury, and related brain disorders. *Biochim. Biophys. Acta Proteom* **2020**, *1868*, 140428. [[CrossRef](#)] [[PubMed](#)]
4. Ding, X.; Ye, N.; Qiu, M.; Guo, H.; Li, J.; Zhou, X.; Yang, M.; Xi, J.; Liang, Y.; Gong, Y.; et al. Cathepsin B is a potential therapeutic target for coronavirus disease 2019 patients with lung adenocarcinoma. *Chem. Biol. Interact.* **2022**, *353*, 109796. [[CrossRef](#)]
5. Yadati, T.; Houben, T.; Bitorina, A.; Shiri-Sverdlov, R. The Ins and Outs of Cathepsins: Physiological Function and Role in Disease Management. *Cells* **2020**, *9*, 1679. [[CrossRef](#)] [[PubMed](#)]
6. Lim, I.T.; Meroueh, S.O.; Lee, M.; Heeg, M.J.; Mobashery, S. Strategy in inhibition of cathepsin B, a target in tumor invasion and metastasis. *J. Am. Chem. Soc.* **2004**, *126*, 10271–10277. [[CrossRef](#)]
7. Ward, C.; Kuehn, D.; Burden, R.E.; Gormley, J.A.; Jaquin, T.J.; Gazdoui, M.; Small, D.; Bicknell, R.; Johnston, J.A.; Scott, C.J.; et al. Antibody targeting of cathepsin S inhibits angiogenesis and synergistically enhances anti-VEGF. *PLoS ONE* **2010**, *5*, e12543. [[CrossRef](#)]
8. Schenker, P.; Alfarano, P.; Kolb, P.; Cafilisch, A.; Baici, A. A double-headed cathepsin B inhibitor devoid of warhead. *Protein Sci.* **2008**, *17*, 2145–2155. [[CrossRef](#)]
9. Turk, V.; Stoka, V.; Vasiljeva, O.; Renko, M.; Sun, T.; Turk, B.; Turk, D. Cysteine cathepsins: From structure, function and regulation to new frontiers. *Biochim. Biophys. Acta* **2012**, *1824*, 68–88. [[CrossRef](#)]
10. Susic, I.; Mirkovic, B.; Arenz, K.; Stefane, B.; Kos, J.; Gobec, S. Development of new cathepsin B inhibitors: Combining bioisosteric replacements and structure-based design to explore the structure-activity relationships of nitroxoline derivatives. *J. Med. Chem.* **2013**, *56*, 521–533. [[CrossRef](#)]
11. Zhu, X.; Wang, H.; Zheng, L.; Zhong, Z.; Li, X.; Zhao, J.; Kou, J.; Jiang, Y.; Zheng, X.; Liu, Z.; et al. Upconversion nanoparticle-mediated photodynamic therapy induces THP-1 macrophage apoptosis via ROS bursts and activation of the mitochondrial caspase pathway. *Int. J. Nanomedicine* **2015**, *10*, 3719–3736. [[CrossRef](#)] [[PubMed](#)]
12. Wang, J.; Yi, J. Cancer cell killing via ROS: To increase or decrease, that is the question. *Cancer Biol. Ther.* **2008**, *7*, 1875–1884. [[CrossRef](#)]
13. Chen, Z.; Woodburn, K.W.; Shi, C.; Adelman, D.C.; Rogers, C.; Simon, D.I. Photodynamic therapy with motexafin lutetium induces redox-sensitive apoptosis of vascular cells. *Arterioscler. Thromb. Vasc. Biol.* **2001**, *21*, 759–764. [[CrossRef](#)] [[PubMed](#)]
14. Jain, M.; Zellweger, M.; Wagnieres, G.; van den Bergh, H.; Cook, S.; Giraud, M.N. Photodynamic therapy for the treatment of atherosclerotic plaque: Lost in translation? *Cardiovasc. Ther.* **2017**, *35*, e12238. [[CrossRef](#)] [[PubMed](#)]
15. Waksman, R.; McEwan, P.E.; Moore, T.I.; Pakala, R.; Kolodgie, F.D.; Hellings, D.G.; Seabron, R.C.; Rychnovsky, S.J.; Vasek, J.; Scott, R.W.; et al. PhotoPoint photodynamic therapy promotes stabilization of atherosclerotic plaques and inhibits plaque progression. *J. Am. Coll. Cardiol.* **2008**, *52*, 1024–1032. [[CrossRef](#)] [[PubMed](#)]
16. Hajri, A.; Wack, S.; Meyer, C.; Smith, M.K.; Leberquier, C.; Keding, M.; Aprahamian, M. In vitro and in vivo efficacy of photofrin and pheophorbide a, a bacteriochlorin, in photodynamic therapy of colonic cancer cells. *Photochem. Photobiol.* **2002**, *75*, 140–148. [[CrossRef](#)]
17. Baskaran, R.; Lee, J.; Yang, S.G. Clinical development of photodynamic agents and therapeutic applications. *Biomater. Res.* **2018**, *22*, 25. [[CrossRef](#)]
18. Xodo, L.E.; Rapozzi, V.; Zacchigna, M.; Drioli, S.; Zorzet, S. The chlorophyll catabolite pheophorbide a as a photosensitizer for the photodynamic therapy. *Curr. Med. Chem.* **2012**, *19*, 799–807. [[CrossRef](#)]
19. Djalil, A.D.; Nurulita, N.A.; Limantara, W.L.; Ibrahim, S.; Tjahjono, D. Biological evaluations of protoporphyrin ix, pheophorbide a, and its 1hydroxyethyl derivatives for application in photodynamic therapy. *Int. J. Pharm. Pharm. Sci.* **2012**, *4*, 741–746.
20. Radestock, A.; Elsner, P.; Gitter, B.; Hipler, U.C. Induction of apoptosis in HaCaT cells by photodynamic therapy with chlorin e6 or pheophorbide a. *Skin. Pharmacol. Physiol.* **2007**, *20*, 3–9. [[CrossRef](#)]
21. Tung, C.H.; Mahmood, U.; Bredow, S.; Weissleder, R. In vivo imaging of proteolytic enzyme activity using a novel molecular reporter. *Cancer Res.* **2000**, *60*, 4953–4958.
22. Choi, Y.; Weissleder, R.; Tung, C.H. Selective antitumor effect of novel protease-mediated photodynamic agent. *Cancer Res.* **2006**, *66*, 7225–7229. [[CrossRef](#)] [[PubMed](#)]
23. Gabriel, D.; Campo, M.A.; Gurny, R.; Lange, N. Tailoring protease-sensitive photodynamic agents to specific disease-associated enzymes. *Bioconjug Chem.* **2007**, *18*, 1070–1077. [[CrossRef](#)] [[PubMed](#)]
24. Herceg, V.; Bouilloux, J.; Janikowska, K.; Allemann, E.; Lange, N. Cathepsin B-Cleavable Cyclopeptidic Chemotherapeutic Prodrugs. *Molecules* **2020**, *25*, 4285. [[CrossRef](#)] [[PubMed](#)]
25. Yu, Z.; Sun, Q.; Pan, W.; Li, N.; Tang, B. A Near-Infrared Triggered Nanophotosensitizer Inducing Domino Effect on Mitochondrial Reactive Oxygen Species Burst for Cancer Therapy. *ACS Nano* **2015**, *9*, 11064–11074. [[CrossRef](#)]
26. Tedjamulia, M.L.; Srivastava, P.C.; Knapp, F.F., Jr. Evaluation of the brain-specific delivery of radioiodinated (iodophenyl)alkyl-substituted amines coupled to a dihydropyridine carrier. *J. Med. Chem.* **1985**, *28*, 1574–1580. [[CrossRef](#)] [[PubMed](#)]

27. Campo, M.A.; Gabriel, D.; Kucera, P.; Gurny, R.; Lange, N. Polymeric photosensitizer prodrugs for photodynamic therapy. *Photochem. Photobiol.* **2007**, *83*, 958–965. [[CrossRef](#)]
28. Ruzza, P.; Quintieri, L.; Osler, A.; Calderan, A.; Biondi, B.; Floreani, M.; Guiotto, A.; Borin, G. Fluorescent, internally quenched, peptides for exploring the pH-dependent substrate specificity of cathepsin B. *J. Pept. Sci.* **2006**, *12*, 455–461. [[CrossRef](#)] [[PubMed](#)]
29. Cho, D.I.; Kim, M.R.; Jeong, H.Y.; Jeong, H.C.; Jeong, M.H.; Yoon, S.H.; Kim, Y.S.; Ahn, Y. Mesenchymal stem cells reciprocally regulate the M1/M2 balance in mouse bone marrow-derived macrophages. *Exp. Mol. Med.* **2014**, *46*, e70. [[CrossRef](#)]
30. Zhang, L.; Chan, C. Isolation and enrichment of rat mesenchymal stem cells (MSCs) and separation of single-colony derived MSCs. *J. Vis. Exp.* **2010**, *37*, e1852. [[CrossRef](#)]
31. Zuluaga, M.F.; Sekkat, N.; Gabriel, D.; van den Bergh, H.; Lange, N. Selective photodetection and photodynamic therapy for prostate cancer through targeting of proteolytic activity. *Mol. Cancer Ther.* **2013**, *12*, 306–313. [[CrossRef](#)] [[PubMed](#)]
32. Gabriel, D.; Lange, N.; Chobaz-Peclat, V.; Zuluaga, M.F.; Gurny, R.; van den Bergh, H.; Busso, N. Thrombin-sensitive dual fluorescence imaging and therapeutic agent for detection and treatment of synovial inflammation in murine rheumatoid arthritis. *J. Control Release* **2012**, *163*, 178–186. [[CrossRef](#)] [[PubMed](#)]
33. Jensen, E.C. Quantitative analysis of histological staining and fluorescence using ImageJ. *Anat. Rec. (Hoboken)* **2013**, *296*, 378–381. [[CrossRef](#)] [[PubMed](#)]
34. Harris-Love, M.O.; Seamon, B.A.; Teixeira, C.; Ismail, C. Ultrasound estimates of muscle quality in older adults: Reliability and comparison of Photoshop and ImageJ for the grayscale analysis of muscle echogenicity. *PeerJ* **2016**, *4*, e1721. [[CrossRef](#)] [[PubMed](#)]
35. Jain, M.; Singh, A.; Singh, V.; Barthwal, M.K. Involvement of interleukin-1 receptor-associated kinase-1 in vascular smooth muscle cell proliferation and neointimal formation after rat carotid injury. *Arterioscler. Thromb. Vasc. Biol.* **2015**, *35*, 1445–1455. [[CrossRef](#)]
36. Jain, M.; Dhanesha, N.; Doddapattar, P.; Nayak, M.K.; Guo, L.; Cornelissen, A.; Lentz, S.R.; Finn, A.V.; Chauhan, A.K. Smooth Muscle Cell-Specific PKM2 (Pyruvate Kinase Muscle 2) Promotes Smooth Muscle Cell Phenotypic Switching and Neointimal Hyperplasia. *Arterioscler. Thromb. Vasc. Biol.* **2021**, *41*, 1724–1737. [[CrossRef](#)]
37. Borle, F.; Radu, A.; Fontolliet, C.; van den Bergh, H.; Monnier, P.; Wagnieres, G. Selectivity of the photosensitizer Tookad for photodynamic therapy evaluated in the Syrian golden hamster cheek pouch tumour model. *Br. J. Cancer* **2003**, *89*, 2320–2326. [[CrossRef](#)]
38. Rapozzi, V.; Zorzet, S.; Zacchigna, M.; Drioli, S.; Xodo, L.E. The PDT activity of free and pegylated pheophorbide a against an amelanotic melanoma transplanted in C57/BL6 mice. *Investig. New Drugs* **2013**, *31*, 192–199. [[CrossRef](#)]
39. He, J.; Wang, Y.; Missinato, M.A.; Onuoha, E.; Perkins, L.A.; Watkins, S.C.; St Croix, C.M.; Tsang, M.; Bruchez, M.P. A genetically targetable near-infrared photosensitizer. *Nat. Methods* **2016**, *13*, 263–268. [[CrossRef](#)]
40. Jain, M.; Zellweger, M.; Frobert, A.; Valentin, J.; van den Bergh, H.; Wagnieres, G.; Cook, S.; Giraud, M.N. Intra-Arterial Drug and Light Delivery for Photodynamic Therapy Using Visudyne(R): Implication for Atherosclerotic Plaque Treatment. *Front. Physiol.* **2016**, *7*, 400. [[CrossRef](#)]
41. Jain, M.; Singh, A.; Singh, V.; Maurya, P.; Barthwal, M.K. Gingerol Inhibits Serum-Induced Vascular Smooth Muscle Cell Proliferation and Injury-Induced Neointimal Hyperplasia by Suppressing p38 MAPK Activation. *J. Cardiovasc. Pharmacol. Ther.* **2016**, *21*, 187–200. [[CrossRef](#)] [[PubMed](#)]
42. Jain, M.; Barthwal, M.K.; Haq, W.; Katti, S.B.; Dikshit, M. Synthesis and pharmacological evaluation of novel arginine analogs as potential inhibitors of acetylcholine-induced relaxation in rat thoracic aortic rings. *Chem. Biol. Drug Des.* **2012**, *79*, 459–469. [[CrossRef](#)] [[PubMed](#)]
43. Zuluaga, M.F.; Gabriel, D.; Lange, N. Enhanced prostate cancer targeting by modified protease sensitive photosensitizer prodrugs. *Mol. Pharm.* **2012**, *9*, 1570–1579. [[CrossRef](#)] [[PubMed](#)]
44. Tang, P.M.; Liu, X.Z.; Zhang, D.M.; Fong, W.P.; Fung, K.P. Pheophorbide a based photodynamic therapy induces apoptosis via mitochondrial-mediated pathway in human uterine carcinosarcoma. *Cancer Biol. Ther.* **2009**, *8*, 533–539. [[CrossRef](#)] [[PubMed](#)]
45. Choi, B.H.; Ryoo, I.G.; Kang, H.C.; Kwak, M.K. The sensitivity of cancer cells to pheophorbide a-based photodynamic therapy is enhanced by Nrf2 silencing. *PLoS ONE* **2014**, *9*, e107158. [[CrossRef](#)]
46. Gabriel, D.; Busso, N.; So, A.; van den Bergh, H.; Gurny, R.; Lange, N. Thrombin-sensitive photodynamic agents: A novel strategy for selective synovectomy in rheumatoid arthritis. *J. Control Release* **2009**, *138*, 225–234. [[CrossRef](#)]
47. Maurer, M.H. Proteomic definitions of mesenchymal stem cells. *Stem Cells Int.* **2011**, *2011*, 704256. [[CrossRef](#)]
48. Sasnouski, S.; Pic, E.; Dumas, D.; Zorin, V.; D’Hallewin, M.A.; Guillemin, F.; Bezdetnaya, L. Influence of incubation time and sensitizer localization on meta-tetra(hydroxyphenyl)chlorin (mTHPC)-induced photoinactivation of cells. *Radiat. Res.* **2007**, *168*, 209–217. [[CrossRef](#)]
49. Kessel, D.; Luo, Y.; Deng, Y.; Chang, C.K. The role of subcellular localization in initiation of apoptosis by photodynamic therapy. *Photochem. Photobiol.* **1997**, *65*, 422–426. [[CrossRef](#)]
50. Jespersen, B.; Tykocki, N.R.; Watts, S.W.; Cobbett, P.J. Measurement of smooth muscle function in the isolated tissue bath—applications to pharmacology research. *J. Vis. Exp.* **2015**, *95*, e52324. [[CrossRef](#)]
51. Wunder, A.; Tung, C.H.; Muller-Ladner, U.; Weissleder, R.; Mahmood, U. In vivo imaging of protease activity in arthritis: A novel approach for monitoring treatment response. *Arthritis. Rheum.* **2004**, *50*, 2459–2465. [[CrossRef](#)] [[PubMed](#)]
52. Yhee, J.Y.; Kim, S.A.; Koo, H.; Son, S.; Ryu, J.H.; Youn, I.C.; Choi, K.; Kwon, I.C.; Kim, K. Optical imaging of cancer-related proteases using near-infrared fluorescence matrix metalloproteinase-sensitive and cathepsin B-sensitive probes. *Theranostics* **2012**, *2*, 179–189. [[CrossRef](#)] [[PubMed](#)]

53. Calfon, M.A.; Rosenthal, A.; Mallas, G.; Mauskopf, A.; Nudelman, R.N.; Ntziachristos, V.; Jaffer, F.A. In vivo near infrared fluorescence (NIRF) intravascular molecular imaging of inflammatory plaque, a multimodal approach to imaging of atherosclerosis. *J. Vis. Exp.* **2011**, *54*, e2257. [[CrossRef](#)] [[PubMed](#)]
54. Liu, L.Y.; Man, X.X.; Yao, H.X.; Tan, Y.Y. Effects of pheophorbide a-mediated photodynamic therapy on proliferation and metastasis of human prostate cancer cells. *Eur. Rev. Med. Pharmacol. Sci.* **2017**, *21*, 5571–5579. [[CrossRef](#)]
55. Yoon, H.E.; Oh, S.H.; Kim, S.A.; Yoon, J.H.; Ahn, S.G. Pheophorbide a-mediated photodynamic therapy induces autophagy and apoptosis via the activation of MAPKs in human skin cancer cells. *Oncol. Rep.* **2014**, *31*, 137–144. [[CrossRef](#)]
56. Satoh, K.; Nigro, P.; Berk, B.C. Oxidative stress and vascular smooth muscle cell growth: A mechanistic linkage by cyclophilin A. *Antioxid. Redox. Signal* **2010**, *12*, 675–682. [[CrossRef](#)]